JOURNAL OF SOLID STATE CHEMISTRY 117, 323–332 (1995)

Metastable Hexagonal Molybdates: Hydrothermal Preparation, Structure, and Reactivity

Jingdong Guo, Peter Zavalij, and M. Stanley Whittingham[1]

Department of Chemistry and Materials Research Center, State University of New York at Binghamton, Binghamton, New York 13902-6000

Received November 21, 1994; accepted November 17, 1994

Hydrothermal treatment of acidified M_2MoO_4 solutions at 150°C for 3 days leads to a range of structures depending on the metal M. Hexagonal molybdates with the general formula $(M_y \cdot zH_2O)$ $Mo_{6-x}O_{18-x}H_{4x-y}$ are formed when M is a small cation, such as Na^+, NH_4^+, and Ag^+. These molybdates crystallize as hexagonal rods and have the space group $P6_3/m$. The open structure of these hexagonal molybdates both allows the M ions in the tunnels to be readily mobile and permits the ready intercalation of additional cations such as hydrogen and lithium. Upon continuous ion exchange of sodium molybdate with 6 N HNO_3, a new hydrate, $MoO_3 \cdot 0.6H_2O$, was formed; subsequent dehydration of this hydrate results in the formation of a new hexagonal modification of "MoO_3." The structural features, thermal properties, diffusion, and reactivity of these phases have been determined and compared with phases synthesized by other methods. © 1995 Academic Press, Inc.

INTRODUCTION

Over the past 2 decades, transition-metal oxides such as WO_3 and MoO_3 have drawn much attention because they form a variety of crystalline phases with open structures, which allow for a rich intercalation chemistry and hence potential application in electrochemical devices. Recently we have been exploring the synthesis of metastable oxides with open crystalline lattices, using mild hydrothermal methods. Although hydrothermal synthesis has been extensively used in the formation of zeolites, and more recently in the preparation of vanadium and molybdenum phosphates, very little work has been reported on the synthesis of transition metal oxides themselves. We previously reported that different crystalline forms of the tungsten(VI) oxides can be readily synthesized using mild hydrothermal methods (1, 2). While extending our work to molybdenum, we found a wide range of products, $M_xMo_yO_3 \cdot nH_2O$, depending on the metal cation M in the reaction medium. When M is a relatively small cation such as Na^+, NH_4^+, and Ag^+, the hexagonal tunnel structure is formed. When larger cations, such as NMe_4^+ or $C_{12}H_{25}N(CH_3)_3^+$, are used, layer structures are formed (3, 4), in addition to Keggin-like cluster compounds. In this paper we discuss the synthesis and characterization of these hexagonal molybdates. The most distinguishing feature of their structure (5) is a wide one-dimensional tunnel (3.2–3.5 Å in diameter) which should allow the ready intercalation of ions. However, there is only a single study that reported that hydrogen could be inserted by "spillover" methods but no details were given (6).

Molybdenum trioxides and their hydrates form a rich family: the well-known thermodynamically stable α-MoO_3 (7), metastable β-MoO_3 phase (8, 9), and various hydrates (10). The MoO_6 octahedron is the basic building unit in all these MoO_3 structures. In orthorhombic α-MoO_3, the MoO_6 octahedra share edges, resulting in a zigzag chain and a unique layer structure (7). β-MoO_3 has a ReO_3-related structure, in which the MoO_6 octahedra share corners to form a monoclinically distorted cube (11). A third form of MoO_3, the so-called hexagonal MoO_3, has been widely reported in the literature (5, 6, 12–20), although it was originally termed "molybdic C-phase" and indexed as cubic (12, 13). It is synthesized by either solid state or solution precipitation methods. The "hexagonal MoO_3" framework is constructed of the same zigzag chains of MoO_6 octahedra as found in α-MoO_3 but they connect through the *cis*-position between chains, as shown in Fig. 1. This structure contains many defects and large cations in the tunnels are thought to be necessary for its stability; its composition is best represented as $MMo_{6-x}[vac]_xH_{6x-1}O_{18}$ (5, 6), where M = K (15), NH_4 (5, 14, 18), $Na \cdot 2H_2O$, K, Rb, Cs, NH_4, and $Ag \cdot 2H_2O$ (19). The molybdenum vacancies in the framework are compensated for by the M cations in the tunnels and by protons attached to the framework oxygen. The structure can also be stabilized by the incorporation of the aliovalent vanadium cation with the ideal formula $KVMo_5O_{18}$; these essentially defect-free compounds are prepared via solid state reaction (16, 17) and recently by an unusual "leaching reaction" (6, 20).

[1] To whom correspondence should be addressed.

0022-4596/95 $12.00
Copyright © 1995 by Academic Press, Inc.
All rights of reproduction in any form reserved.

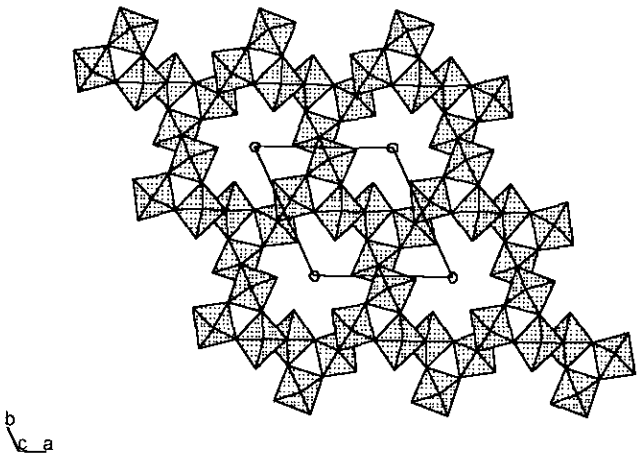

FIG. 1. Structure of hexagonal molybdate $KMo_5O_{15}H_5 \cdot 2H_2O$, viewed from the 001 direction.

EXPERIMENTAL

I. Hydrothermal formation of hexagonal molybdates: A 1 *M* $Na_2MoO_4 \cdot 2H_2O$ (Aldrich, 99.9%) solution was acidified with 3 *M* HCl to pH 1.5, giving a clear green solution which was transferred to a 100-ml Teflon-lined autoclave (Parr 4744), sealed, and reacted hydrothermally for 3 days at 150°C and autogenous pressure. The resulting pale yellow microcrystallites were collected by suction filtration, washed with water, and air dried at 50·C. Similar hydrothermal conditions were used for the ammonium [II] and silver compounds [III]: commercial H_2MoO_4 (Fisher 99%) and concentrated NH_4OH were mixed in the molar ratio of 1 : 4 and the mixture was acidified with HCl to pH 1.5. In the case of silver, Ag_2MoO_4 (from the stoichiometric reaction of $Na_2MoO_4 \cdot 2H_2O$ and $AgNO_3$) was acidified with HNO_3 to pH 1.45. The hexagonal molybdenum trioxide hydrate $(H_3O)_yMoO_3 \cdot zH_2O$ [IV] was obtained by multiple acid treatment of the sodium form [I] with 6 *N* HNO_3 at 60°C. Fresh HNO_3 solution must be replaced every hour; eight to nine successive operations are necessary to achieve the H_3O^+ exchange. The absence of Na^+ in [IV] was indicated by the absence of any residue on thermogravimetric analysis (TGA) up to 1000°C; α-MoO_3 begins to sublime at 790°C. An Electron Microprobe (JEOL 2000) confirmed that there was no detectable sodium. Upon dehydration of this hexagonal MoO_3 hydrate [IV] at 270–300°C under oxygen atmosphere, a new hexagonal "MoO_3" with empty tunnels was formed (21).

II. Chemical analyses and characterization. ICP atomic emission was used for elemental analyses; the water content was determined from TGA (Perkin–Elmer TG-7) and the ammonium content by the Keldjahl method. SEM was used for morphological observation; powder X-ray diffraction (XRD), was used for phase identification, and TGA/DSC was used for thermal properties. FTIR was also used for supplemental information. The densities of the molybdates were determined volumetrically by gas displacement (22) as 3.86 ± 0.1, 3.73 ± 0.1, and 4.28 ± 0.02 g/cc for the sodium, ammonium, and silver compounds, respectively.

III. ac impedance. The sample, as previously described (23), was pressed into a pellet, 0.5 cm^2 in area and 0.1 cm thick, coated with silver paste on both sides, and measured in a tube furnace in air. A GenRad 1693 RLC Digibridge instrument was used and the measurement frequency ranged from 10 Hz to 200 KHz; the applied voltage was 0.1 V. The conductivity values were obtained from the intercepts of the complex impedance plot with the real axis.

IV. Lithium intercalation. A weighed sample was dehydrated and vacuum dried for 1 hr prior to lithiation. An excess amount of *n*-butyllithium in hexane (1.6 *M*, Adrich Chemical) was added to the sample and allowed to react overnight. After three to four rinses with hexane, the excess lithium was back titrated with standard HCl to give the degree of lithiation.

V. Rietveld refinement. XRD measurements were made on a Scintag XDS 2000 X-ray powder diffractometer using CuK_α radiation. For Rietveld analysis, data was collected over the 2θ range 8–140°, step scan 0.02° interval and pulse time 20–30 sec. A CSD (crystal structure determination) software package (24) was used for cell parameter refinement and Rietveld analysis.

VI. Electrochemical intercalation. A two-electrode system was applied with the lithium anode strip also acting as the reference electrode; the cathodes were hexagonal molybdates, and 2 *M* $LiClO_4$ in 1,3-dioxolane was used as the electrolyte. The cathode was prepared by mixing the active material (30–100 mg) with carbon black and Teflon powder at 50, 30, and 20% by weight, respectively, and then hot-pressing (5 ton pressure, 270°C) onto a nickel grid. Before being transferred into a Braun helium-filled dry box, the sample was heated under vacuum to remove residual water. Discharge/charge of cell was performed by a Mac Pile II electrochemical system.

RESULTS AND DISCUSSION

Hydrothermal treatment of acidified M_2MoO_4 solution yielded a single molybdate phase with a light color (white with greenish tint for Na and NH_4, and yellow for Ag). Figure 2 shows SEM images of the sodium and silver forms; the solid is well crystallized and the hexagonal symmetry is evident. Their XRD patterns were indexed to hexagonal unit cell with space group $P6_3/m$. These XRD patterns were similar to those prepared by other methods (5). Chemical analysis gave the *A*/Mo as 0.19 : 1

for Na, 0.2 for Ag, 0.22 : 1 for NH_4, approximately one A ion per hexagonal tunnel site as shown in Fig. 1. The water content depends on the identity of the cation, varies slightly with the conditions of preparation, and is lost on heating as shown in the TGA curves in Fig. 3. Since hydrothermal reactions usually lead to the highest oxidation state in the case of tungsten and molybdenum oxides, the oxidation state of Mo in these molybdates is assumed to be +6, which is evidenced by their light color. According to density measurements, a molybdenum defect model (to be discussed further in text) best describes these compositions as $(A_y \cdot zH_2O)Mo_{6-x}O_{18-x}(H)_{4x-y}$, where $y \approx 1$, $0.3 < x < 0.5$, and z can be up to 2; the hydrogen might be bound as hydroxyl or as hydronium. The composition and cell parameters of these molybdates are shown in Table 1. These are similar to the ones prepared by solution precipitation methods (5, 19) but with lower water contents, and slightly different A/Mo ratios and thus different vacancy concentrations, which can be attributed to the different preparation methods.

Recently we reported (21) that the continuous ion exchange reaction of the sodium compound [I] with 6 N HNO_3 gave a white (pale white with a greenish tint) powder which retains the hexagonal structure. TGA of this hydrate [IV] exhibited a continuous weight loss up to 260°C and no break was observed between adsorbed water and crystalline water (Fig. 3). DSC showed a broad endothermic peak corresponding to the loss of water and a sharp exothermic peak around 370°C, indicating a phase change. This is the first report on the formation of MoO_3 hydrate with no metallic cation or ammonium in the hexagonal tunnels, thus adding one member to the already-rich family of MoO_3 hydrates (10). An X-ray study showed that after the complete dehydration of [IV], empty tunnel MoO_3 [V] retains the hexagonal structure up to 360°C, when it transforms to the more stable α-MoO_3. Hu *et al.* (6) also prepared the empty tunnel structure by acid exchange of $Na_{0.13}V_{0.13}Mo_{0.87}O_3$, but in this case the structure is stabilized to higher temperatures by the presence of the vanadium.

We also attempted to obtain this open hexagonal MoO_3 by thermally decomposing the ammonium compound [II]; however, after the final loss of ammonium (410°C from TGA and DSC), the hexagonal MoO_3 transforms irreversibly to the more stable α-MoO_3, in agreement with Caiger *et al.* (5). This phase transformation occurs for the sodium [I] and silver compounds [III] at 380 and 340°C, respectively. This hexagonal MoO_3 [V] is of interest due to its microporosity and possible catalytic activity, and many attempts to prepare it by the deammoniation of $NH_4VMo_5O_{18}$ (19) or $(NH_4)_{0.13}V_{0.13}Mo_{0.87}O_3$ (5) failed. The temperature for deammoniation (at least 420°C) is far higher than the transformation temperature of hexagonal MoO_3 (340–380°C in our observation); therefore, our successful preparation of open hexagonal MoO_3 [V] might be associated with the much lower temperature of dehydration, 260°C. Another key point is that the dehydration must be carried out in an oxygen environment, as under vacuum or in inert environments the various hexagonal molybdates are reduced, leading to the formation of molybdenum bronzes. The bronze formation was evidenced by the color changing to gray and by the ability of this gray product to be oxidized by 0.1 N aqueous $Ce(SO_4)_2$ solution. Mo remains in the Mo(VI) state, while in an oxygen environment. This bronze formation may be represented by

$$(A_y \cdot zH_2O)Mo_{6-x}O_{18-x}(H)_{4x-y} \xrightarrow{-H_2O,\ -O_2} \text{“}A_yMoO_3\text{.”}$$

A similar type of redox reaction has been found in potassium tungstates and 123-superconductor (25), but it is not yet fully understood how the oxygen diffuses out of the hexagonal tunnel.

Some key structural information was deduced from the FTIR spectra, which are shown in Fig. 4 for the ammonium molybdate [II]. The most important feature is a relatively sharp band at 970 cm^{-1}, characteristic of the stretching of Mo=O double bond (9), which is also found in orthorhombic α-MoO_3 indicating a terminal oxygen in the framework (9). The existence of bending vibration band of H–O–H at 1624 cm^{-1} proves that the crystalline water is coordinated as H_2O molecules, the band at 3457 cm^{-1} is assigned as –OH stretching from H_2O or hydroxyl and the bands below 1000 cm^{-1} are assigned as O–Mo–O stretching and bending with different Mo–O bond lengths. Other molybdates showed bands similar to those of [II] except for the bands at 3195 and 1400 cm^{-1}, which are characteristic of the ammonium ion.

The structure of hexagonal MoO_3 was determined by Darriet and Galy (16) for $K_{0.13}V_{0.13}Mo_{0.87}O_3$ and by Krebs and Paulat-Boschen (15) for the so-called potassium decamolybdate $KMo_5O_{18}H_5$. The framework shows some relation to the hexagonal tungsten bronze K_xWO_3, having the basic segment of three corner-sharing MO_6 octahedra. In the bronze, these octahedra share only corners and form a six-member ring stacking along the c axis, resulting in space group $P6/mmm$ or $P6/mcm$, while in $KMo_5O_{18}H_5$ (or $K_{0.13}V_{0.13}Mo_{0.87}O_3$), half of the three-member segments shift 1/4 along the c axis and join to the neighboring segment by edge-sharing, leading to the structure with space group $P6_3/m$ (see Fig. 1). In $K_{0.13}V_{0.13}Mo_{0.87}O_3$, the unit cell contains 6 Mo (or V) and 18 O atoms on the 6(h) sites and 6x K^+ ions are distributed over the 2(b) sites. $KMo_5O_{18}H_5$ has the same framework but in this case the Mo atoms occupy only five-sixths of the 6(h) sites and potassium occupies half the 2(b) sites in the large hexagonal tunnels of Fig. 1. The charge imbalance caused by

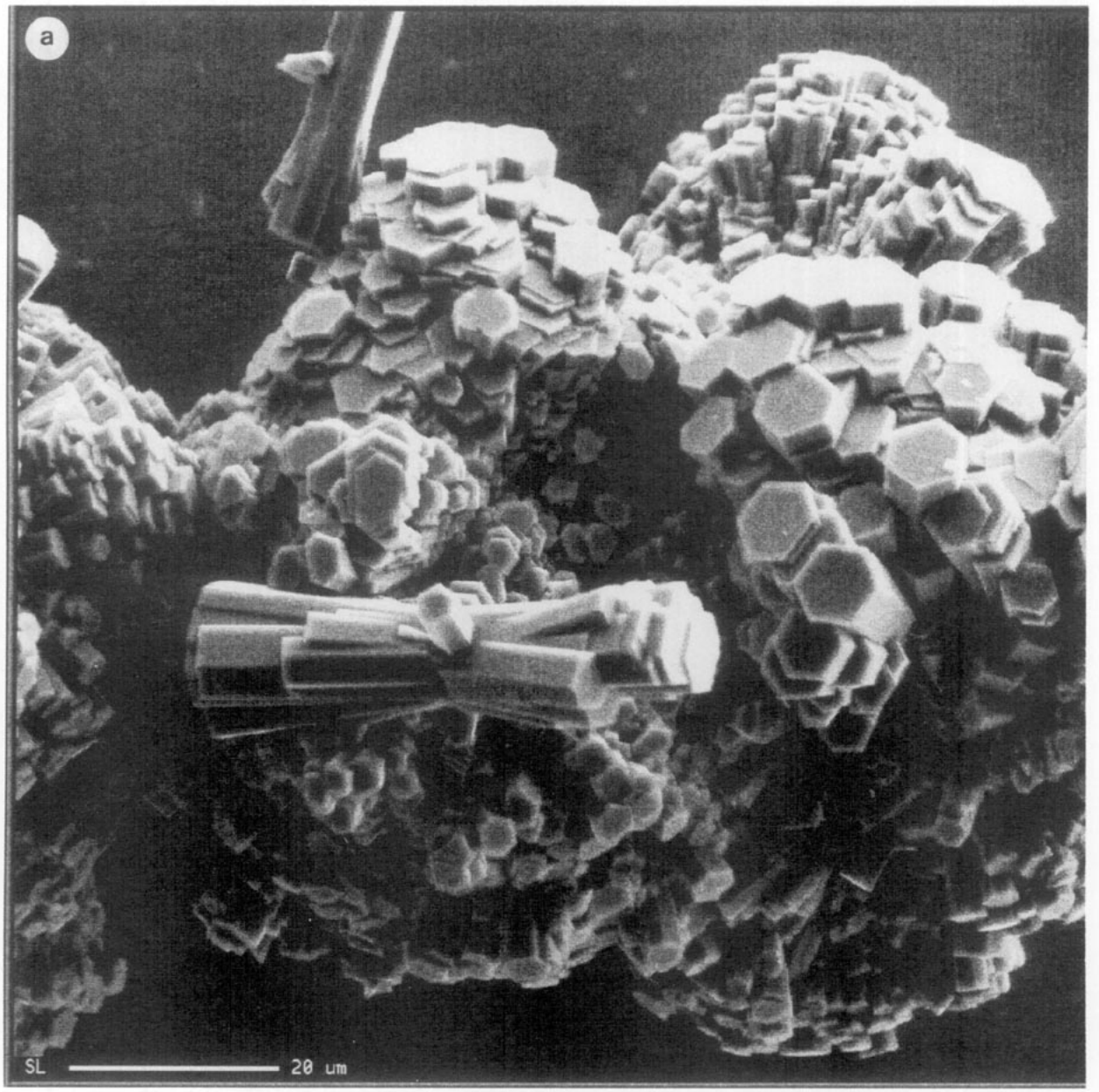

FIG. 2. SEM images of (a) sodium molybdate and (b) silver molybdate.

the molybdenum vacancy can be compensated for by the presence of K^+ and H^+ in the structure. Although the existence and exact location of H are not proved, they are probably attached to oxygen associated with the molybdenum vacancy (15). McCarron *et al.* also determined the structure of $(Na \cdot 2H_2O)Mo_{5.33}[H_{4.5}]_{0.67}O_{18}$ (19) and found that the shift of Na^+ from the 2(*b*) sites was due to the two extra water molecules per unit cell being accommodated within the channels; in addition two molybdenum vacancies per three cells were found, rather than one per cell in $KMo_5O_{18}H_5$.

In order to further reveal the structural detail of as-synthesized molybdates, Rietveld analysis of these samples was carried out. We adopted the atomic coordinates of $KMo_5O_{18}H_5$ as a starting model, the space group chosen for the refinement was $P6_3/m$, and precise hexagonal unit cell dimensions of samples were obtained by a least-squares fit of the XRD pattern. At the beginning, only

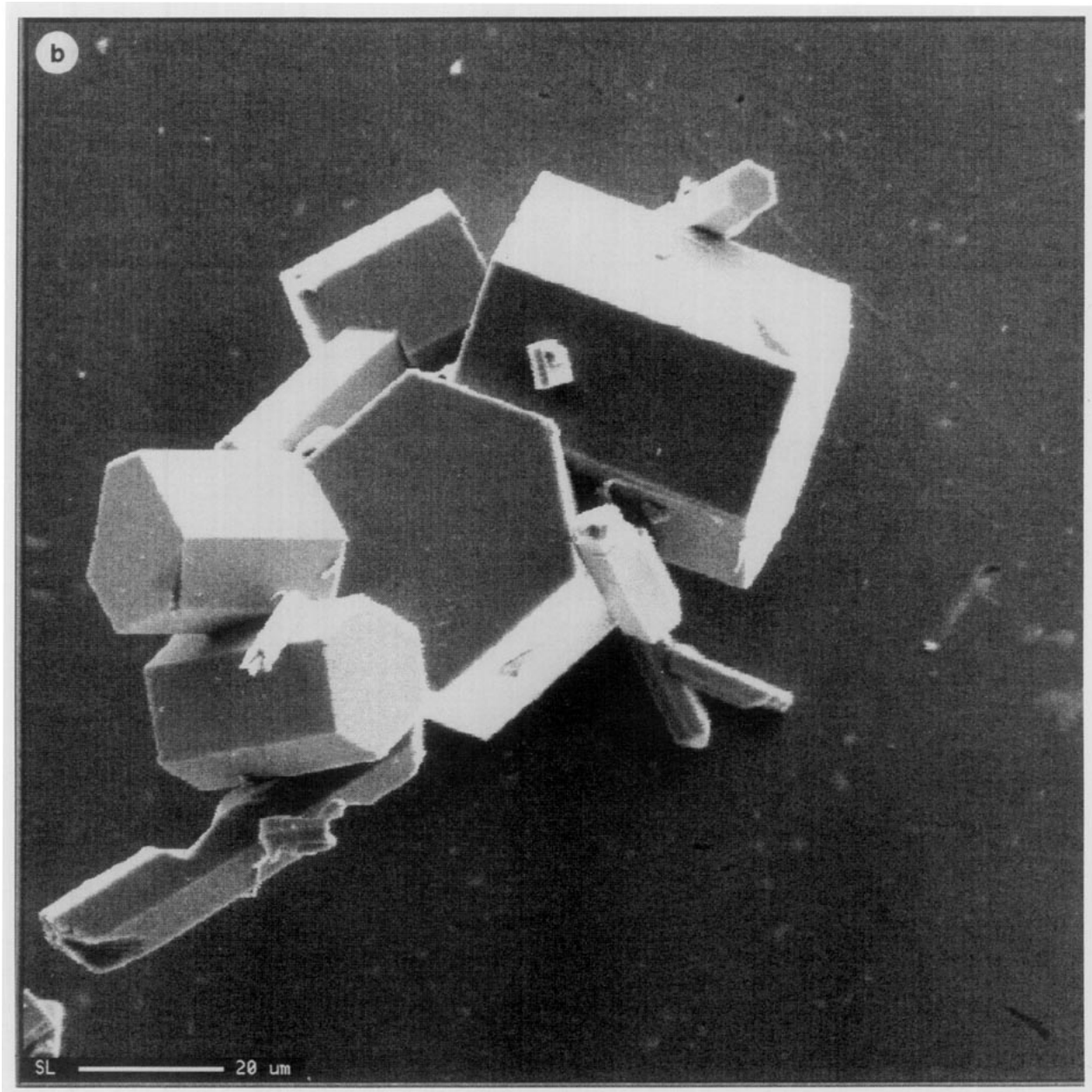

FIG. 2—*Continued*

framework $MoO(3)_{3/3}O(2)_{2/3}O(1)_{1/1}$ were placed; the number here indicates that oxygen is being shared by 3 (edge), 2 (corner), and 1 (terminal) octahedra and the bondlengths are around 1.7, 1.9, and 2.2 Å, respectively. After refining the profile parameters, a difference Fourier search was applied and the cations were gradually added as the refinement proceeded. Attempts were also made to determine the nature of the charge compensation. For fully oxidized molybdates or tungstates, which usually are found in the hydrothermal products, two models were considered: Mo vacancy as in $M_yMo_{1-x}O_3$ and oxygen interstitials as in $M_xMoO_{3+x/2}$, in which the framework is free of molybdenum vacancies but extra O^{2-} along with water must be placed in the tunnels to balance the charge of M cations. The second model has been found in the case of $Na_xWO_{3+x/2}$ (25). We refined both models and found that the R factor did not change significantly and Mo–O bond lengths and chemical compositions refined

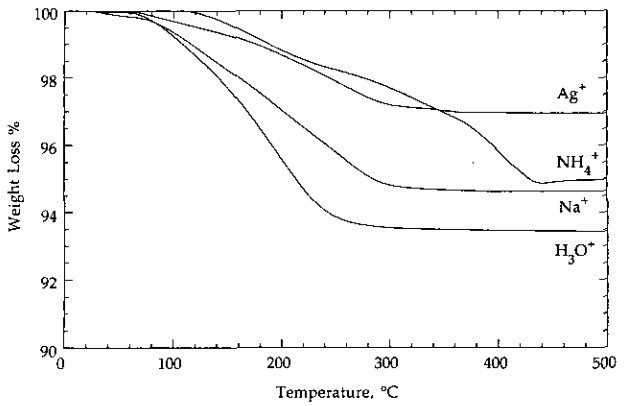

FIG. 3. TGA curves of hexagonal molybdates under helium.

to similar values. This shows that the two models are virtually indistinguishable from X-ray powder data and neutron data would be necessary to locate the H atom and consequently distinguish H_2O (or H_3O^+) and O^{2-} in the tunnels. However, according to our density measurements, a molybdenum-defect model agrees better with experimental values; therefore, final refinements were made based on the molybdenum-defect model. The defect model was also used for $KMo_5O_{18}H_5$ (15) and $(Na \cdot 2H_2O)$ $Mo_{5.33}[H_{4.5}]_{0.67}O_{18}$ (19), where only the molybdenum occupancy was refined while the framework oxygens' occupancy remained constant. Here we propose that if the terminal oxygen atom O(1) is only bonded to Mo, it would be more reasonable to fix its occupancy to the same value as Mo. Final structural parameters are listed in Table 2 and the observed and difference profiles of the silver molybdates is shown in Fig. 5.

The framework consists of hexagonal MoO_3, as in $KMo_5O_{18}H_5$, and the cations are disordered along the 001 tunnel axis. Attempts at placing A^+ at one of $(x, y, 1/4)$ or $(0, 0, 0)$ did not improve or lower the R factor, indicating that A^+ ions are disordered along the (001) direction. The relatively large thermal parameter B also suggests the cations are delocalized along the hexagonal tunnels. Although water and cations are not distinguished in Table 2, some of the M' and M'' in Table 2 are water molecules. The water content is approximately half of the value determined from the chemical composition. The remaining water is believed to be water adsorbed on the surface; a similar discrepancy was reported for $WO_3 \cdot 1/3H_2O$ and for $Na_xWO_{3+x/2}$ (25) and was also attributed to adsorbed water.

Important bond lengths and angles are listed in Table 2. As can be seen, the Mo–O bond lengths refined to 1.65–1.75, 1.97, and 2.30 Å respectively, which fall well within in the range of Mo–O bond lengths. The distances of A cations (or water) and O(1) are 2.4–3.1 Å which also agree well with O–cation or hydrogen-bonded O–O distances.

Of particular interest in these open structure compounds is the possible diffusion of cations in the tunnels. To study the diffusion behavior, we performed ac impedance measurements on those samples. Figure 6 shows $\log(\sigma T)$ vs $T/1000$ plots of as-synthesized molybdates. The Ag, Na, and NH_4 compounds exhibit the normal linear increase with increasing temperature, with the conductivity being $Ag^+ \approx Na^+ > NH_4^+$ at low temperature and approaching the same at elevated temperature. Molybdenum trioxide hydrate [IV] shows a behavior similar to that observed earlier for the pyrochlore $WO_3 \cdot nH_2O$ (23): the conductivity decrease above 140°C is believed to be caused by the loss of water from the tunnels. The facile diffusion of sodium out of the tunnels during ion exchange is not difficult to understand. Sodium must move past the H_2O molecules to leave the structure, and there is ample space for this motion considering the large tunnel dimension (≈3.5 Å in diameter). The much faster diffusion rate for H_3O^+ than Na^+ might be explained by the unique Grotthuss-type of mechanism for the hydronium H_3O^+ ion. At 24°C the conductivity of the protonic species is 3.5×10^{-7} S/cm. If we assume that all the ions are mobile, then the diffusion coefficient is 2 ×

TABLE 1
Composition, Density, and Cell Parameters of Hexagonal Molybdenum Oxides

Compounds	Chemical composition[a]	Measured density (g/cc)	Cal. density defect		Cell parameters		
			Mo	O^{2b}	a (Å)	c (Å)	Volume
Na [I]	$Na_{1.0}Mo_{5.35}O_{17.35}H_{1.6} \cdot 1.7H_2O$	3.86	3.86	4.46	10.624(1)	3.726(1)	364.23
NH_4 [II]	$(NH_4)_{\approx 1}Mo_{5.3}O_{17.3}H_{1.7} \cdot 0.4H_2O$	3.73	3.73	4.31	10.533(1)	3.729(1)	358.26
Ag [III]	$Ag_{\approx 1}Mo_{5.5}O_{17.5}H_{1.0} \cdot 1.1H_2O$	4.28	4.28	4.87	10.601(1)	3.727(1)	362.70
H_3O [IV]	$H_{1.0}Mo_{5.35}O_{17.35}H_{1.6} \cdot 1.7H_2O$	—	3.74	4.32	10.584(1)	3.728(1)	361.64

[a] From density and TGA results, based on Mo vacancy model.
[b] The two defects considered are molybdenum vacancies and oxygen interstitials; the latter assumes 100% occupancy on the molybdenum site.

TABLE 2
Crystallographic Data[a] (Atomic Position and Bond Lengths)

		Ag	Na	NH_4	H_2O
a (Å)		10.6007(1)	10.6242(1)	10.5332(1)	10.5840(6)
c (Å)		3.7269(1)	3.7261(1)	3.7286(1)	3.7278(3)
V (Å^3)		362.70(1)	364.23(1)	358.26(1)	361.642(7)
d_{calc} (g/cc)		4.3035(2)	3.8324(1)	3.7224(1)	3.7061(1)
d_{exp} (g/cc)		4.28	3.86	3.73	3.72
R(Bragg) (%)		4.7	4.0	3.7	3.9
R(prof) (%)		6.3	6.3	5.3	7.5
Rw(prof) (%)		7.7	8.1	8.9	10.1
			Atomic parameters		
Mo	x	0.3558(1)	0.3562(2)	0.3550(2)	0.3550(2)
	y	0.4605(1)	0.4602(1)	0.4580(1)	0.4583(2)
	z	1/4	1/4	1/4	1/4
	B (Å^2)	0.89(3)	0.73(8)	0.58(2)	1.00(5)
	g	0.920	0.92(1)	0.882(7)	0.875
O(1)	x	0.2626(8)	0.2631(8)	0.2633(7)	0.2672(7)
	y	0.2759(8)	0.2732(9)	0.2746(8)	0.2756(7)
	z	1/4	1/4	1/4	1/4
	B (Å^2)	1.1(3)	0.7(3)	0.7(3)	1.6(2)
	g	0.920	0.92(1)	0.882(7)	0.875
O(2)	x	0.2149(9)	0.2204(10)	0.2093(8)	0.2125(7)
	y	0.4953(8)	0.5040(9)	0.5013(7)	0.4947(6)
	z	1/4	1/4	1/4	1/4
	B (Å^2)	2.1(4)	2.7(3)	2.2(3)	1.2(2)
O(3)	x	0.5923(8)	0.5811(7)	0.5816(6)	0.5791(6)
	y	0.5081(10)	0.5015(9)	0.5053(8)	0.4943(8)
	z	1/4	1/4	1/4	1/4
	B (Å^2)	1.2(2)	0.8(2)	0.5(2)	2.1(2)
M'	x	−0.0014(12)	0.085(3)	0	0
	y	0.0967(10)	0.021(4)	0	0
	z	1/4	1/4	1/4	1/4
	B (Å^2)	3.2(2)	6.2(8)	2.9(9)	1.1(7)
	g[b]	0.134(2)	0.257(7)	0.472(7)	0.37(2)
M''	x	0			0
	y	0			0
	z	0.074(15)			0
	B (Å^2)	6.0(9)			0.7(7)
	g[c]	0.056(8)			0.31(2)
			Distances		
Mo–O(1)		1.695(7)	1.721(8)	1.673(7)	1.675(7)
O(2)		1.709(11)	1.722(12)	1.806(10)	1.733(8)
O(3)		1.924(2)	1.952(3)	1.953(2)	1.965(2)
O(3)		2.297(10) *2	2.204(9) *2	2.181(8) *2	2.207(8) *2
O(2)		2.387(8)	2.361(9)	2.289(7)	2.389(6)
M'–O(1)		2.475(15)	2.39(4)	2.835(7) *3	2.873(7) *3
		2.54(2)	2.71(4)		
		2.608(9) *2	2.78(3) *2		
M''–O(1)		2.931(15) *3			3.021(7) *6
		3.10(2) *3			

[a] Space group $P6_3/m$, and lattice parameters from Rietveld refinement.
[b] Occupancy factor for metal in site $6h$.
[c] Occupancy factor for metal in site $4c$.

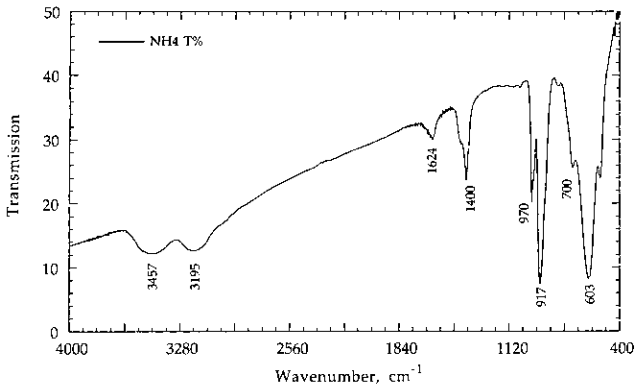

FIG. 4. FTIR of ammonium molybdate.

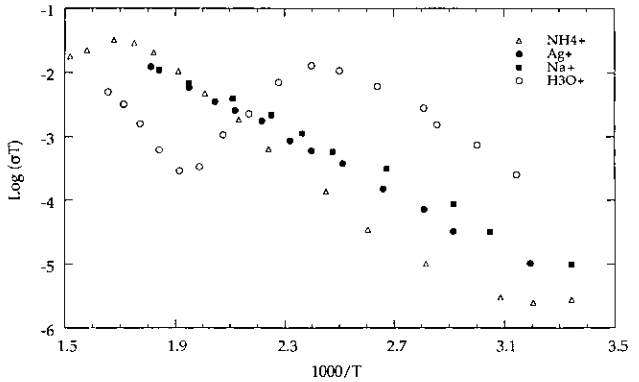

FIG. 6. Ionic conductivity of hexagonal molybdates.

10^{-11} cm^2/sec; this value is two orders of magnitude lower than in the pyrochlore $WO_3 \cdot nH_2O$, but still is comparable to that in the hexagonal HTBs (26). Again, it is easy to perceive, in pyrochlore structure, that H_3O^+ ions can move through interconnected 3-D tunnels so that some blockages in one dimension are not that important to overall diffusion.

As might be expected, all these hexagonal molybdates readily undergo a variety of insertion reactions. The reactions of [I]–[IV] with Zn/HCl occur immediately and blue molybdenum bronzes $M_yH_xMoO_3$ resulted; there was minimal lattice change; thus after hydrogen insertion the lattice parameters of the sodium and ammonium compounds were a = 10.770 Å, c = 3.727 Å and a = 10.553 Å, c = 3.731 Å, respectively. However, in the case of the silver compound, silver metal precipitated out. The reactions of the various hexagonal phases with n-butyllithium lead to dark blue to black compounds of varying lithium content. Table 3 lists the lithiation data of these hexagonal molybdates, as well as the changes in the unit cell on drying and after the subsequent lithiation. Reaction of the empty structure results in a 0.7 Li/Mo ratio, to give a hexagonal lattice with a = 10.559 Å and c = 3.725 Å. This corresponds to a 1% volume contraction while the sodium and ammonium compounds exhibit an increase of 1.5 and 0.7%, respectively.

Both the empty hexagonal MoO_3 [V] and the dehydrated sodium compound [I] incorporated similar amounts of lithium. This suggests that lithium does not reside on 2(a) or 2(b) sites in the tunnels, but probably prefers the triangular prismatic sites as in $Li_yK_xWO_3$ and $Li_{1.8-1.9}Na_{0.26}WO_{3.13}$ (2) and some other small sites in the tunnels. The ammonium compound reacts with slightly more lithium than the sodium phase, which might be due to some reduction of the NH_4^+ ion. The silver compound reacts with the most lithium (1.75 Li/Mo), which might be associated with the formation of metallic silver but structural characterization is not possible due to the amorphous nature of the product. This phenomenon was also observed for the silver pyrochlore tungstates (2). The chemical reversibility of the lithiation reaction was demonstrated by reaction with a Br_2/CH_3CN mixture; the

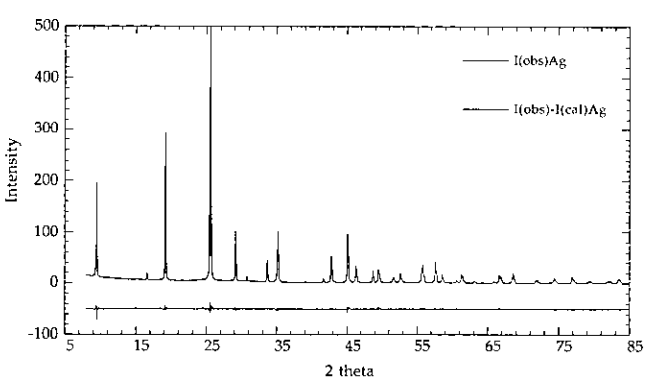

FIG. 5. Rietveld profile of silver molybdate, showing the observed and difference plots.

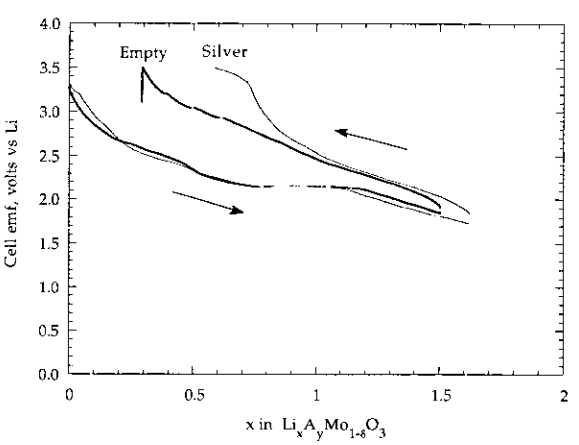

FIG. 7. Electrochemical cycling curves of empty and silver hexagonal molybdates.

TABLE 3
Lithium Intercalation of Hexagonal Molybdates

As-synthesized oxide	Dehydrated oxide	After lithiation	% Volume change
[I] $Na_{1.0}Mo_{5.35}O_{17.35}H_{1.6} \cdot 1.7H_2O$ a = 10.624(1), c = 3.726(1) Å Volume = 364.19 Å^3	"$Na_{0.2}MoO_{3.1}$" a = 10.541(4), c = 3.713(3) Å Volume = 357.3 Å^3	$Li_{0.6-0.7}$"$Na_{0.2}MoO_{3.1}$" a = 10.576(4), c = 3.744(2) Å Volume = 362.7 Å^3	+1.5%
[II] $(NH_4)_{\approx 1}Mo_{5.3}O_{17.3}H_{1.7} \cdot 0.4H_2O$ a = 10.533(1), c = 3.729(1) Å Volume = 358.26 Å^3	"$(NH_4)_{0.2}MoO_{3.1}$" a = 10.569(1), c = 3.721(1) Å Volume = 359.96 Å^3	$Li_{0.95}$"$(NH_4)_{0.2}MoO_{3.1}$" a = 10.581(6), c = 3.739(4) Å Volume = 362.53 Å^3	+0.71%
[III] $Ag_{\approx 1}Mo_{5.5}O_{17.5}H_{1.0} \cdot 1.1H_2O$ a = 10.601(1), c = 3.727(1) Å Volume = 362.7 Å^3	"$Ag_{0.2}MoO_{3.1}$" a = 10.596(4), c = 3.728(2) Å Volume = 362.49 Å^3	$Li_{1.7}$"$Ag_{0.2}MoO_{3.1}$" Amorphous/few peaks	
[IV] $H_{1.0}Mo_{5.35}O_{17.35}H_{1.6} \cdot 1.7H_2O$ a = 10.584(1), c = 3.728(1) Å Volume = 361.63 Å^3	"MoO_3" a = 10.619(1), c = 3.719(1) Å Volume = 363.2 Å^3	$Li_{0.7}$"MoO_3" a = 10.559(5), c = 3.725(3) Å Volume = 359.7 Å^3	+0.97%

compounds changed from black to blue after 1 week's reaction, indicating that bromine is not a sufficiently strong oxidizing agent to allow the complete removal of lithium.

The electrochemical lithiation of these hexagonal molybdates was performed in a molybdate/Li^+/Li cell. Discharge curves at a current density of 30 μA/cm^2 with a cut-off voltage of 1.7 V are shown in Fig. 7. All the molybdates exhibit similar discharge behaviors. The cell voltage generally shows a continuous decrease as the degree of lithiation increased. However, there is an indication of a plateau around $x = 0.7$ suggestive of a two-phase region; this is at the same composition as the maximum chemical lithiation observed for empty MoO_3. This behavior is not dissimilar to that observed in α-MoO_3, where close to 1.5 Li/Mo can be realized (27), but no clear plateau was found. Kumagai *et al.* (28) observed a similar amorphization for the molybdic acid C phase when x exceeded 1.0. As can be seen from Fig. 7, a high cell polarization is observed on charge. This suggests that the kinetics of Li diffusion out of the structure is slow, which might be associated with some structural changes; less likely, electron transfer might be rate limiting. The charge curves encountered a barrier at ca. $x \approx 0.7$ for the silver and sodium compounds; charging was better for the empty structure. More experiments on charge/discharge cycling of these cells, determination of the lithium diffusion coefficient, and XRD studies are underway to reveal the structural detail of these compounds during cycling.

After the completion of this work, it was reported that hydrogen and lithium could be intercalated into the vanadium–molybdenum trioxide structure to give $(H,Li)_xV_{0.13}Mo_{0.87}O_3$, and that the structure was degraded if x exceeded unity (29).

CONCLUSIONS

Mild hydrothermal synthesis of molybdate solutions in the presence of small cations such as sodium, silver, and ammonium leads to the hexagonal molybdenum trioxide structure. The cations are readily mobile in the structure, with the hydronium ion showing the greatest conductivity. On dehydration of the hydronium compound formed by the acidification of the sodium molybdate, an empty tunnel structure is formed. The lattice readily undergoes reduction by the intercalation of hydrogen and lithium, with little change in the structure. Optimization of the reversibility of the lithium reaction could lead to their use in lithium batteries.

ACKNOWLEDGMENTS

We thank the Department of Energy for support of this research through Lawrence Berkeley Laboratory. Thanks are also due to Frank DiSalvo of Cornell University for the loan of the density device.

REFERENCES

1. K. P. Reis, A. Ramanan, and M. S. Whittingham, *Chem. Mater.* **2,** 219 (1990).
2. J.-D. Guo and M. S. Whittingham, *Int. J. Mod. Phys. B* **7,** 4145 (1993).
3. M. S. Whittingham, J. Li, J.-D. Guo, and P. Zavalij, *in* "Soft Chemistry Routes to New Materials. Nantes, France, 1993." *Mater. Sci. Forum* **152–153,** 99 (1994).
4. J. Guo, P. Zavalij, and M. S. Whittingham, *Chem. Mater.* **6,** 357 (1994).
5. N. A. Caiger, S. Crouch-Baker, P. G. Dickens, and G. S. James, *J. Solid State Chem.* **67,** 369 (1987).
6. Y. Hu, P. K. Davies, and T. P. Feist, *Solid State Ionics* **53–56,** 539 (1992).
7. G. Andersson and A. Magneli, *Acta Chem. Scand.* **4,** 793 (1950).
8. E. M. McCarron, *J. Chem. Soc. Chem. Commun.*, 336 (1986).

9. M. Figlarz, *Prog. Solid State Chem.* **19,** 1 (1989).
10. R. L. Fellows, M. H. Lloyd, J. F. Knight, and H. L. Yakel, *Inorg. Chem.* **22,** 2468 (1983).
11. J. B. Parise, E. M. McCarron, R. V. Dreele, and J. A. Goldstone, *J. Solid State Chem.* **93,** 193 (1991).
12. M. L. Freedman and S. Leber, *J. Less-Common Met.* **7,** 427 (1964).
13. H. Peters, L. Till, and K. H. Radeke, *Z. Anorg. Allg. Chem.* **365,** 14 (1969).
14. N. Sotani, *Bull. Chem. Soc. Jpn.* **48,** 1820 (1975).
15. V. B. Krebs and I. Paulat-Boschen, *Acta Crystallogr. Sect. B* **32,** 1697 (1976).
16. B. Darriet and J. Galy, *J. Solid State Chem.* **8,** 189 (1973).
17. I. P. Olenkova, L. M. Plyasova, and S. D. Kirik, *React. Kinet. Catal. Lett.* **16,** 81 (1981).
18. L. Garin and J. M. Blanc, *J. Solid State Chem.* **58,** 98 (1985).
19. E. M. McCarron, D. M. Thomas, and J. C. Calabrese, *Inorg. Chem.* **26,** 370 (1987).
20. T. P. Feist and P. K. Davies, *Chem. Mater.* **3,** 1011 (1991).
21. J. Guo, P. Zavalij, and M. S. Whittingham, *Eur. J. Solid State Chem.* **31,** 833 (1994).
22. M. Y. Chern, R. D. Mariani, D. A. Vennos, and F. J. DiSalvo, *Rev. Sci. Instrum.* **61,** 1733 (1990).
23. J.-D. Guo, K. P. Reis, and M. S. Whittingham, *Solid State Ionics* **53–56,** 305 (1992).
24. L. G. Akselrud, Y. N. Grin, Y. P. Zavalij, V. K. Pecharsky, and V. S. Fundamenskii, CSD—Universal program package for single crystal and/or powder structure data treatment. *In* "12th European Crystallographic Meeting. Moscow, 1989."
25. K. P. Reis, E. Prince, and M. S. Whittingham, *Chem. Mater.* **4,** 307 (1992).
26. K. H. Cheng, A. J. Jacobson, and M. S. Whittingham, *Solid State Ionics* **5,** 355 (1981).
27. J. O. Besenhard, J. Heydecke, and H. P. Fritz, *Solid State Ionics* **6,** 215 (1982).
28. N. Kumagai, N. Kumagai, and K. Tanno, *Electrochim. Acta* **32,** 1521 (1987).
29. Y. Hu and P. K. Davies, *Mater. Sci. Forum* **152–153,** 277 (1994).